Enhancing the fill-factor of CMOS SPAD arrays using microlens integration

G. Intermite*[a], R. E. Warburton [a], A. McCarthy [a], X. Ren [a], F. Villa [b], A. J. Waddie [a], M.R. Taghizadeh [a], Y. Zou [b], F. Zappa [b], A. Tosi [b] and G. S. Buller [a]

[a] Institute of Photonics and Quantum Sciences, Heriot-Watt University, Edinburgh, EH14 4AS, UK; [b] Politecnico di Milano, Dipartimento di Elettronica, Informazione e Bioingegneria, p. Leonardo Da Vinci 32, 20133 Milano, Italy

ABSTRACT

Arrays of single-photon avalanche diode (SPAD) detectors were fabricated, using a 0.35 µm CMOS technology process, for use in applications such as time-of-flight 3D ranging and microscopy. Each 150 x 150 µm pixel comprises a 30 µm active area diameter SPAD and its associated circuitry for counting, timing and quenching, resulting in a fill-factor of 3.14%. This paper reports how a higher effective fill-factor was achieved as a result of integrating microlens arrays on top of the 32 x 32 SPAD arrays. Diffractive and refractive microlens arrays were designed to concentrate the incoming light onto the active area of each pixel. A telecentric imaging system was used to measure the improvement factor (IF) resulting from microlens integration, whilst varying the f-number of incident light from f/2 to f/22 in one-stop increments across a spectral range of 500-900 nm. These measurements have demonstrated an increasing IF with f-number, and a maximum of ~16 at the peak wavelength, showing a good agreement with theoretical values. An IF of 16 represents the highest value reported in the literature for microlenses integrated onto a SPAD detector array. The results from statistical analysis indicated the variation of detector efficiency was between 3-10% across the whole f-number range, demonstrating excellent uniformity across the detector plane with and without microlenses.

Keywords: CMOS SPAD array, SPAD imager, diffractive microlens.

1. INTRODUCTION

Many applications require detectors with single-photon sensitivity in the visible and near infrared (400 – 850 nm) wavelength region[1–4]. In this spectral range, detection of weak optical signals can be achieved using standard complementary metal-oxide-semiconductor (CMOS) Image Sensors incorporating linear-mode avalanche photodiodes (APDs)[5,6]. APDs operating in linear mode, however, do not have sufficient internal gain to detect single-photons. For this reason, single-photon detectors such as photomultiplier tubes (PMTs), microchannel plates, superconducting single-photon detectors, and single-photon avalanche diodes (SPADs) have been developed to satisfy requirements in terms of single-photon sensitivity and picosecond timing resolution[7]. Among the various choices, silicon SPADs are preferred because of their intrinsic advantages typical of solid state devices, such as low power consumption, miniature size, low bias voltages, operation at room temperature, reduced magnetic field susceptibility, reliability, and low cost[8–10].

Si SPADs are essentially silicon p-n junctions, and are reverse biased above the breakdown voltage by a voltage known as excess bias (V_{EX}), in the so called Geiger-mode of operation. In this state, the electric field is sufficiently high (> 3 x 10^5 V/cm) that a single carrier injected in the depletion layer can trigger a self-sustaining avalanche, which gives rise to a macroscopic current pulse in the milliampere range[7,9,11]. If the primary carrier is photo-generated, the leading edge of the avalanche pulse marks (with picosecond jitter) the arrival time of the detected photon. Once the avalanche has been triggered, the current continues to flow until the avalanche is quenched by lowering the bias below the breakdown voltage. After quenching, a suitable circuitry is used to bring the p-n junction back to the initial state of above-breakdown biasing, in order to detect another photon[10,12].

Si SPADs can be mainly divided in two groups, depending on the thickness of the depletion layer of the p-n junction, which can be thin[13], typically thickness of approximately 1 µm, or thick[14], typically 20 µm or more. The choice of the depletion layer thickness depends on the performance required by a specific application.

*gi23@hw.ac.uk; www.single-photon.com

When fabricated from custom technologies Si SPADs have a spectral efficiency tailored to the wavelength of interest, and provide the best performance in terms of dark counts and afterpulsing[15,16]. However, such custom fabrication technology cannot be easily used to integrate on-chip complex electronics, potentially affecting the performance of these devices in terms of afterpulsing, optical crosstalk, power consumption, large module size, high cost, and limiting the number of pixels to tens or hundreds. These problems have led researchers to explore the design of monolithically integrated single-photon imaging system fabricated by high-voltage (HV) and standard deep sub-micron (DSM) CMOS technologies, which have been demonstrated by different research groups[17–21]. By using CMOS technology, a very high level of on-chip integration is possible, allowing incorporation of complex digital processing circuits within SPAD pixels. Several applications are now pursued using SPAD arrays including fluorescence lifetime maps of various fluorophores[22–24]; 3-D images using light detection and ranging (LIDAR)[25,26]; as well as for other applications demanding single-photon sensitivity in the visible wavelength range combined with a high frame rate.

One disadvantage of SPAD arrays implemented in standard CMOS technology is the limited fill-factor (which is the ratio of photo-sensitive area to overall focal plane array area), due to the requirement of guard rings and the placement of in-pixel electronics[27]. Reduction in fill-factor implies deterioration of the photon detection efficiency (PDE), since a larger fraction of incident photons are not detected. Different solutions have been proposed and attempted to recover the loss of sensitivity due to the low fill-factor, such as the use of an array of micro-optical concentrators[28,29] or a 3-D integration technology[30,31]. In the former approach, each pixel has its own micro-optical concentrator, which collects light from the objective plane in the focal plane and directs it to the sensitive area of each pixel in the detector plane, and hence enhancing the fill factor of a SPAD array. The downside of this approach is the increase of fabrication complexity and cost. In the second approach, the in-pixel electronics no longer surround the detector, but are placed on a separate silicon wafer that is either wafer-to-wafer bonded to another wafer containing an array of SPADs or it is connected to the SPAD chip using through-silicon-vias (TSVs). These last techniques have been mainly demonstrated for InGaAsP SPAD arrays which are flip-chip bonded to the CMOS readout integrated circuit[32].

In this paper, we report on the recovery of the fill factor on a 32 x 32 Si CMOS SPADs array[21] by integrating two different sets of 32 x 32 plano-convex infinite and finite conjugate diffractive microlens arrays. Although both sets of microlens were designed for operation at a wavelength of 808 nm, the characterisation was performed in the spectral range of 500-900 nm. By using a custom telecentric imaging system, we measured the improvement factor (IF) resulting from the microlens integration at different f-numbers, and demonstrated the highest IF reported in the scientific literature for microlens integrated on a SPAD array. Finally, we also showed an excellent uniformity for the IF and for both chips with and without microlens, below 10 %, at all f-numbers and across the spectral range under investigation.

2. SPAD-BASED IMAGE SENSORS

The 32 x 32 Si CMOS SPAD array described in this paper was designed and characterized in terms of single-photon performance using measurements such as dark count rate (DCR), PDE and afterpulsing in Ref. [21]. It was processed in a high-voltage 0.35 μm CMOS process. These devices were designed for range imaging based on the Time of Flight (TOF) principle, and were used to calculate the distance between the measurement system and an object by measuring the time taken for a pulse, emitted from the optical source, to travel to the object and back to the detector. A cross-section of a 30 μm active area diameter SPAD along with a simplified representation of the electric field across the device is shown in Figure 1. More information regarding the design of these SPAD detectors can be found in ref. [33].

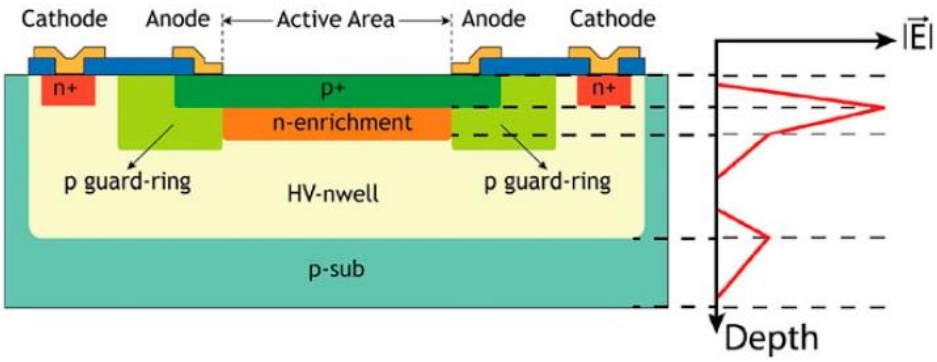

Figure 1. Cross-section of the SPAD developed in 0.35 μm HV CMOS technology and the simplified electric field along the center of the device[33].

The designed camera is based on 32 x 32 "smart' pixel, each containing a SPAD detector, a quenching circuit, a 6 bit counter and an in-pixel 10 bit Time-to-Digital Converter (TDC)[34] to measure the photon arrival time. Figure 2 shows the block diagram of the "smart" pixel with overall dimensions of 150 μm x 150 μm. This corresponds to a fill factor of 3.14 % for the chip with no microlens.

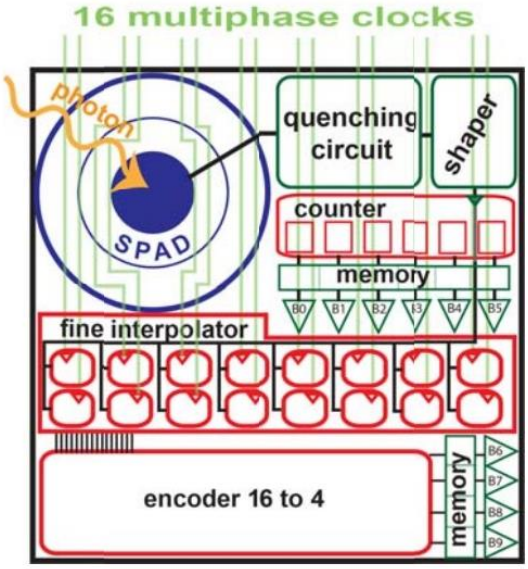

Figure 2. Block diagram of the "smart" pixel for TOF measurements, with overall dimensions of 150 μm x 150 μm, employing a SPAD with active area diameter of 30 μm. The output of the pixel is a 10 bit (for timing information about the TOF measurement) or a 6 bit (for imaging information) digital data bus.

The array of 32 x 32 pixels can operate in both photon timing and photon counting modes. The photon counting mode has been used to perform all the measurements reported in this paper, and pixels have been used to measure the intensity of constant or slowly varying optical signals within a time slot that can be set from 50 ns to 500 ms[34]. In photon counting mode, either a photon absorbed into the SPAD active area or a dark count initiates the avalanche process by producing a macroscopic signal, which is sensed by the quenching circuit. The avalanche is quenched and the counter is incremented. After a well-defined hold-off time, during which photons cannot be detected, the SPAD is reset back to operation, in order to detect other photons. These operations are performed during the whole time duration of a frame and all pixels within each array work independently. The beginning of a frame is marked by sequence of the Stop and Start signals, which are applied in parallel to all pixels of the array. Therefore all accumulated counts are frozen at the same time and are stored into the 1024 in-pixel registers. Data read-out is carried out using a row-column access scheme. The limit for the maximum achievable frame-rate (i.e. the minimum frame duration) is given by the time

necessary to read the whole array. For the array used in this paper, a maximum frame-rate of 100 kframe/s was experimentally measured. More details on smart pixel architecture and operation can be found in ref. [34].

3. MICROLENS ARRAYS

A major drawback to the increasing level of monolithically integrated circuitry is that the relative detection area of the SPAD array is low – as mentioned in the previous section, ~3% of the total area of each "smart" pixel in the array is capable of detecting incident photons. The development of high fill-factor microlens arrays, capable of producing diffraction limited spots at the detector plane, offers a solution to this problem. The two main competing techniques that can be used for the fabrication of microlens arrays are the refractive and diffractive microlenses. The refractive microlens approach potentially offers a greater spectral bandwidth, however they will not afford a full 100% filling of the pixel dimension. Integration of refractive microlens arrays with SPAD arrays are the subject of ongoing work, and will be discussed in more detail in a future publication. The second approach to microlens fabrication is the diffractive lens technique where the lens surface is approximated by a modulo 2π zone plate representation. In this case, the fill-factor will be 100% and, although the lenses are designed to produce a particular focal length at a particular operational wavelength, a diffractive microlens can still produce a focal spot within the SPAD active area over a significant range of wavelengths with a high improvement factor. Figure 3a shows the layout of a part of the 32 x 32 array of microlenses designed to operate at a wavelength of 808 nm. The focal length of the lenses (at λ = 808 nm) was designed to be 1035μm giving a diffraction limited spot size of 13μm and the calculated and measured values (under 780 nm illumination) were 1075μm and 12.5μm, and 1125μm and 12.4μm respectively. Diffractive microlens arrays were used for the results reported in this paper – a fused silica substrate measuring approximately 5.6 x 5.6 mm and containing the 100% fill factor 32 x 32 diffractive microlens array was aligned with, and bonded directly onto, the top surface of the 9 x 9 mm die containing the 32 x 32 array of SPAD detectors. Figure 3b shows a photograph of a fully assembled 32 x 32 Si CMOS SPAD sensor integrating microlens.

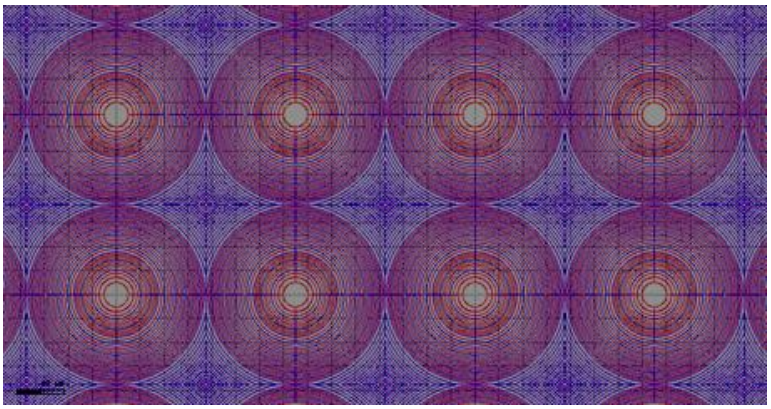

(a)

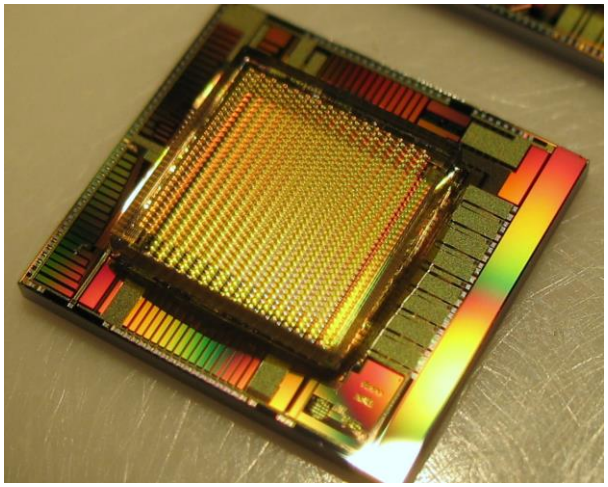

(b)

Figure 3. (a) An image showing part of 32 x 32 microlens array designed for 808nm illumination, and (b) a photograph of a fully assembled 32 x 32 Si CMOS SPAD sensor integrating microlens.

4. EXPERIMENTAL SETUP

To characterize both Si CMOS SPAD arrays, with and without microlenses, the setup shown in Figure 4 was used. A tunable NKT Supercontinuum laser source was used to make measurements of the IF and uniformity in the spectral range between 500 – 900 nm. Light coupled in a single-mode fibre (5 μm diameter core) then diverges upon exiting the fibre and propagates along the optical bench over a length of ~1 meter where it is incident on a diffuser. This diffuser ensured that the near-collimated light is diffused uniformly throughout a large cone angle (~ 50º). This system is composed of two identical converging lenses with an aperture stop placed at the common focal point. Measurements of the IF and uniformity were performed at different f-numbers between f/2 and f/22 at one-stop increments. The SPAD array was mounted on a micrometer three-axis translation stage, and it was placed at a distance f from the rear lens of the telecentric system. All the reported measurements were performed at room temperature and in completely dark conditions. Furthermore, the excess bias voltage on SPAD arrays under test, with and without microlens, was kept fixed at a value of 3 V.

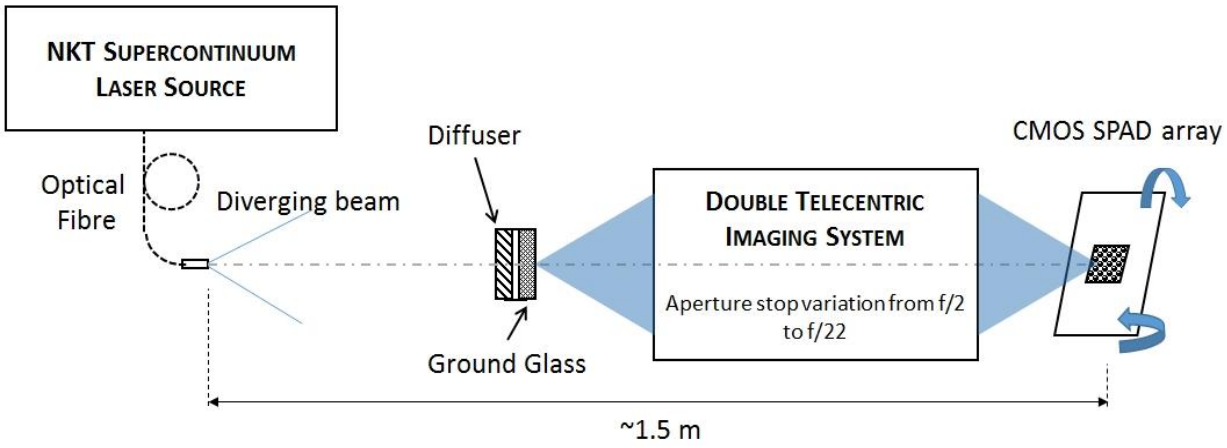

Figure 4. Experimental setup used to evaluate the improvement factor resulting from microlens integration at varying f-numbers. This setup was also used to evaluate the uniformity of SPAD arrays

The optical system described in Fig. 4 guarantees a linear relationship between aperture area and count rate across the range of f-numbers (from f/2 to f/22) and tunable to different wavelengths.

5. IMPROVEMENT FACTOR AND UNIFORMITY

To evaluate the infinite and finite conjugate diffractive microlenses performance resulting from the integration on the 32 x 32 SPAD array, we used the concept of improvement (or concentration) factor proposed in ref. [28]:

$$IF = E_0/E_i \quad (1)$$

where E_i is the input irradiance (optical power per unit area) at the microlens surface, and E_0 is the output irradiance or the irradiance at the photosensitive area of the pixel.

Empirically, the improvement factor is obtained by dividing the detected photon event profile (which is the difference of the light and background signal) on the SPAD array with integrated microlens arrays by the detected photon profile measured by the SPAD array with no integrated microlens, under the same illumination conditions. As mentioned above, the IF was measured in the spectral range between 500 and 900 nm. Hence the improvement factor at a given f-number was the results of two measurements, which were performed for each sensor, with and without microlenses, one illuminated and another in complete darkness. Before calculating the IF, the hot pixels were removed and their values were calculated using the median filter method at their corresponding location. Hot pixels are defined as those SPADs with a DCR much higher than the average value of the best (i.e. those with lower DCR). The SPAD arrays used in this paper showed less than a 5% proportion of hot pixels (see Fig. 10 of ref. [33]).

Figure 5 shows a comparison for the average improvement factor calculated at different wavelengths for both chips integrating two different set of microlenses. All the measurements were performed at a fixed f/number equal to f/16.

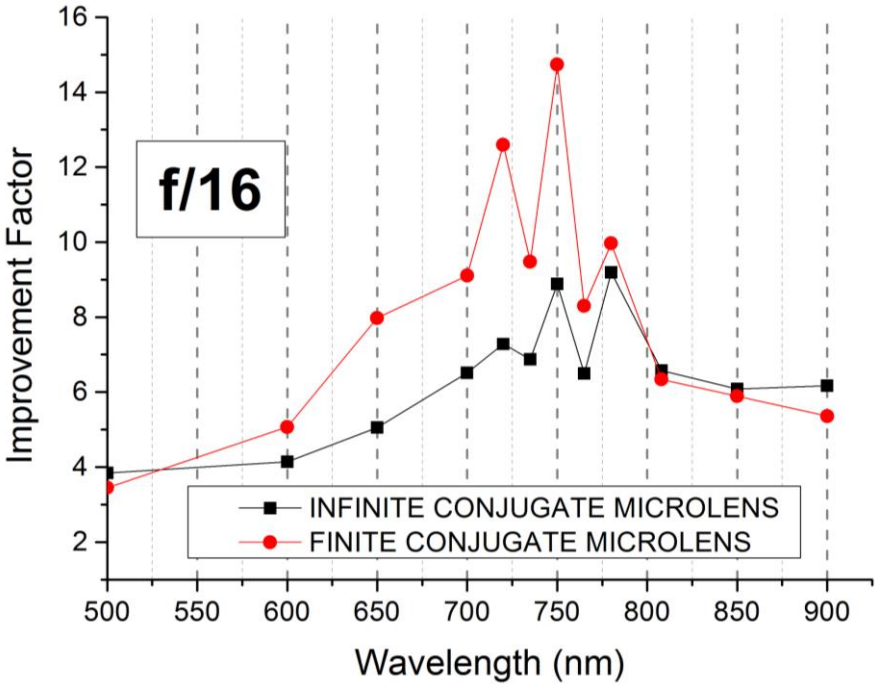

Figure 5. Comparison of the average improvement factor calculated experimentally in the spectral range of interest (from 500 to 900 nm) for both infinite (black line and square) and finite (red line and circle) conjugate diffractive microlenses. The aperture was kept fixed to f/16.

In particular, the IF measured for the infinite conjugate microlens array exhibited a maximum value of 10.5 at a wavelength of 780 nm (Fig. 5). For the finite conjugate microlens, the maximum value of 15.5 was obtained at a wavelength of 750 nm. At the design wavelength (808 nm), the IF had similar values of 5.8 and 6.3 for the infinite and finite microlenses, respectively. We believe that the design wavelength of 808 nm was shifted to slightly shorter wavelengths, 780 nm and 750 nm, for the infinite and finite conjugate diffractive microlenses respectively, due to fabrication tolerance errors.

Therefore, the IF was measured at the peak wavelength for both infinite and finite microlenses, as illustrated in Figure 6a-b. Both graphs show the comparison of the IF, at 750 and 780 nm, as a function of the f-number ranging from f/2 to f/22 with one-stop increment.

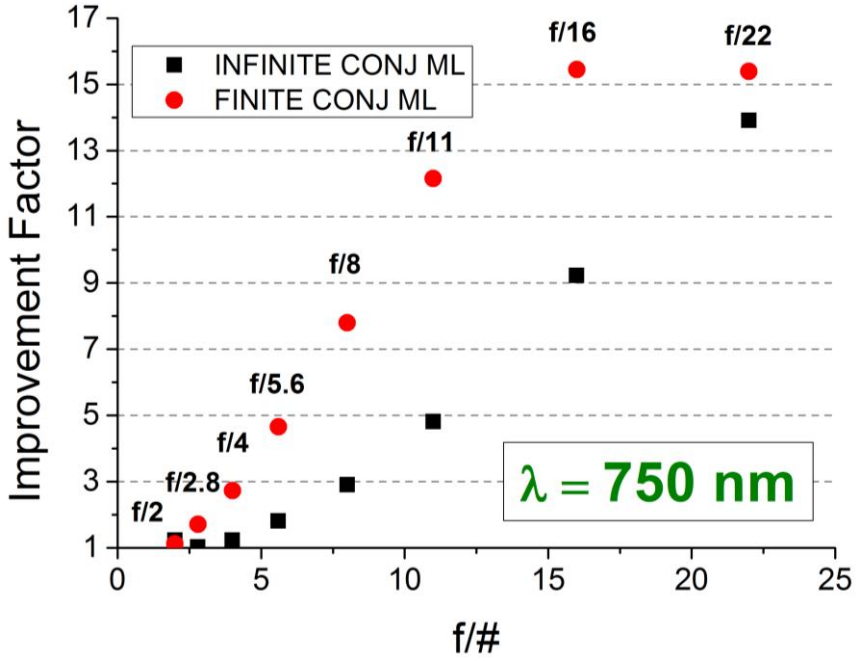

(a)

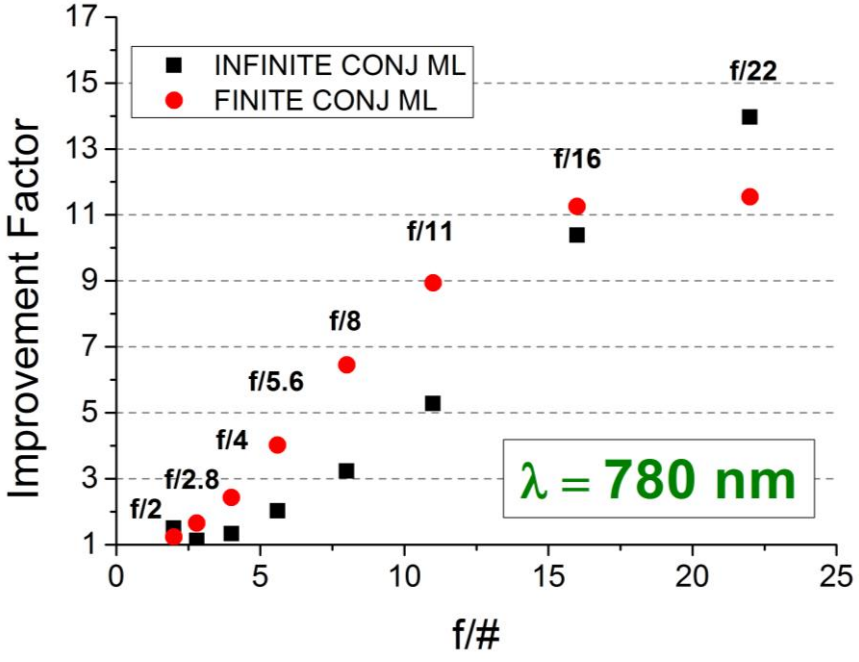

(b)

Figure 6. Comparison of the average improvement factor at a wavelength of (a) 750 nm, and (b) 780 nm for both sets of microlenses measured at various f-numbers from f/2 to f/22 with a one-stop increment.

Results showed that, at both wavelengths, the IF of the finite conjugate microlens is higher than the IF measured for the infinite conjugate microlens at low f/numbers, from f/4 to f/11 (Figure 6). This was expected because the finite conjugate

microlens array substrate is designed for a source placed at finite distance from the microlens. On the other hand, the design of the infinite conjugate microlens substrate is optimized for light from a source placed at infinity. Hence at high f-numbers it is expected that the infinite conjugate will perform better.

Another important parameter to evaluate during the characterization of a SPAD array is the spatial uniformity of detection, and to ascertain any degradation due to integration of the microlens arrays. This parameter was evaluated by considering the coefficient of variation (CV) defined as the ratio of the standard deviation (σ) to the mean (μ) expressed in percentage. For the measurements under investigation, the CV aimed to describe the variability, and hence the uniformity, of the measured light intensity and the IF across the whole sensor.

Figure 7 shows the measured light intensity (which is the difference between signal and background) in 10 frames on all three SPAD sensors (bare chip, infinite and finite conjugate diffractive microlens). All the images were taken under the same light condition, at a wavelength of 750 nm and with an aperture equal to f/16.

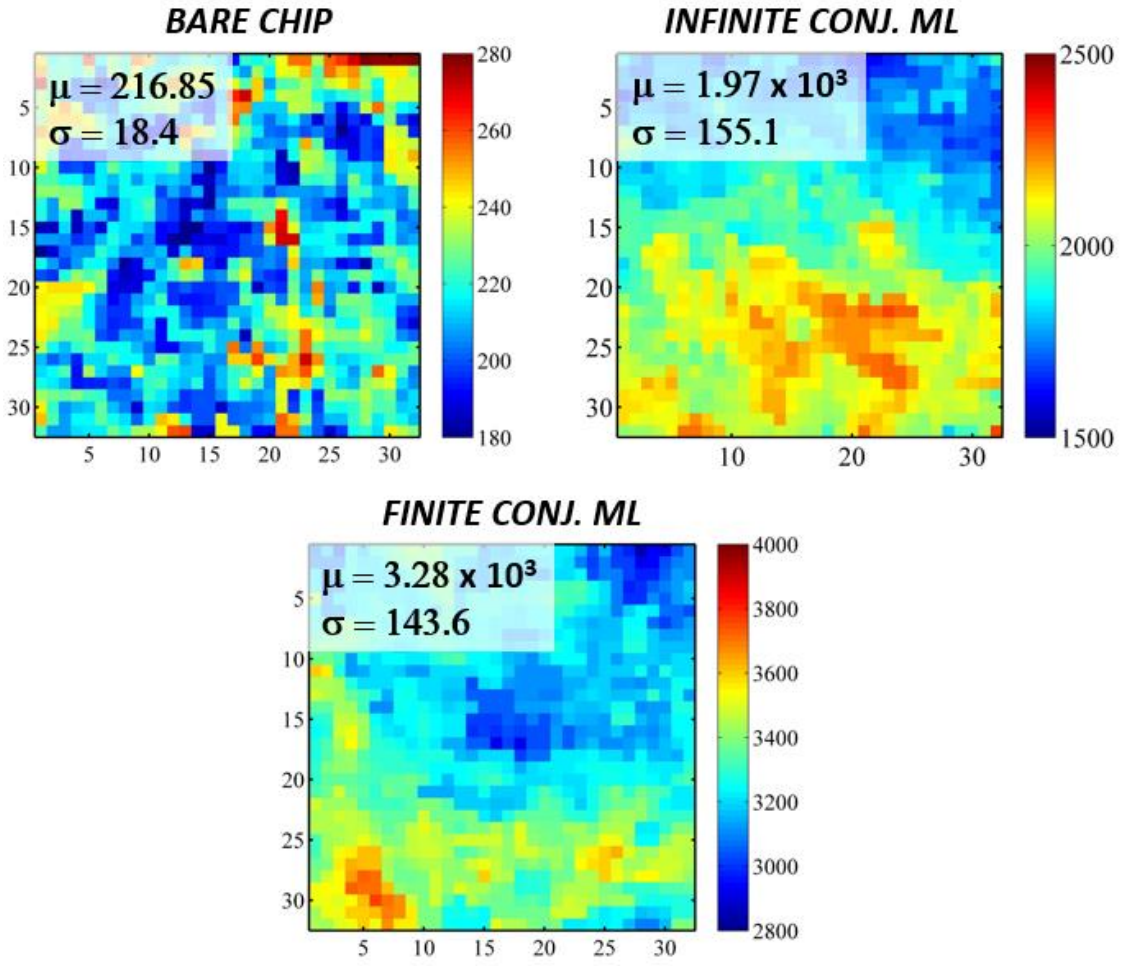

Figure 7. Light intensity (which is the difference between signal and background) images obtained for each of the three SPAD arrays (bare chip, infinite and finite conjugate diffractive microlens) under the same light condition, at a wavelength of 750 nm and aperture stop equal to f/16. The value of mean (μ) and standard deviation (σ) are also reported for all images. A CV of 8.5 %, 7.8%, and 4.3% was obtained for the bare chip, infinite and finite conjugate, respectively.

For each images shown in Figure 7, the scale intensity for each array was adapted to enhance the visibility of the images because of the different improvement factors of each array, and hence higher number of counts. In fact, the increase in light intensity due to the microlens integration is clearly visible. For each array the value of mean and standard deviation are reported in Figure 7, demonstrating a CV of 8.5 %, 7.8%, and 4.3% for the bare chip, infinite and finite conjugate,

respectively. In general, the uniformity was less than 10% at all f-numbers, with higher value of the CV at the highest f/number (f/16 and f/22) for which the telecentric error became significant.

The uniformity of the IF was also calculated for both arrays integrating infinite and finite microlens, as illustrated in Figure 8, where the IF has been color coded. In this case, the same color scale was used for the improvement factor images in order to highlight the different improvement for both arrays with microlenses. The calculated CV was equal to 11.5% and 9.12% for the infinite and finite microlens, respectively.

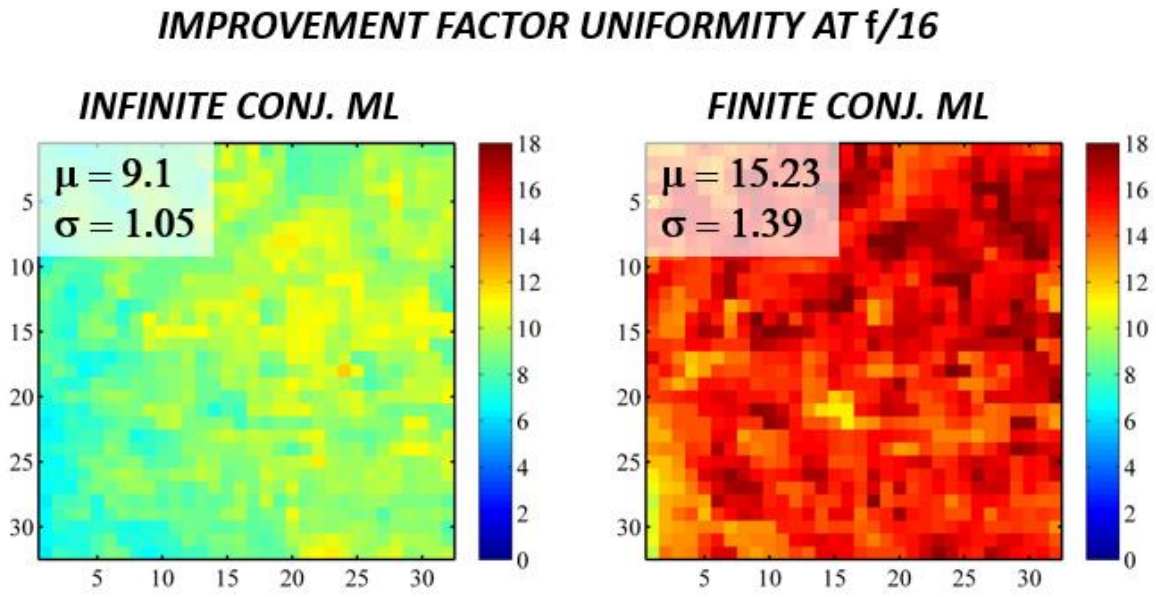

Figure 8. Improvement factor images obtained with SPAD arrays integrating the infinite (left) and finite (right) conjugate diffractive microlenses at a wavelength of 750 nm and aperture stop equal to f/16. The value of mean and standard deviation are also reported for all images.

6. CONCLUSION

We have integrated diffractive microlens arrays and achieved improvements factors of up to 15. The integration shows no discernable degradation in the uniformity performance of the arrays, indicating excellent optical alignment in the integrated package. The IF reduces with decreasing f-number as expected and ongoing work will investigate optimized designs for more effective operation at low f-numbers, including the use of refractive microlens arrays.

ACKNOWLEDGMENTS

The team acknowledges the support of the EU FP7 project "MiSPiA" (Grant Agreement Number 257646). The team from Heriot-Watt University is affiliated to the Scottish Universities Physics Alliance (SUPA) and acknowledges support from the UK Engineering and Physical Sciences Research Council (Platform Grant Award: EP/F048041/1).

REFERENCES

[1] Gariepy, G., Krstajić, N., Henderson, R., Li, C., Thomson, R. R., Buller, G. S., Heshmat, B., Raskar, R., Leach, J., et al., "Single-photon sensitive light-in-flight imaging," Nat. Commun. **6** (2015).

[2] McCarthy, A., Ren, X., Della Frera, A., Gemmell, N. R., Krichel, N. J., Scarcella, C., Ruggeri, A., Tosi, A.., Buller, G. S., "Kilometer-range depth imaging at 1550 nm wavelength using an InGaAs/InP single-photon avalanche diode detector," Opt. Express **21**(19), 22098–22113 (2013).

[3] Wallace, A. M., McCarthy, A., Nichol, C. J., Ren, X., Morak, S., Martinez-Ramirez, D., Woodhouse, I. H.., Buller, G. S., "Design and Evaluation of Multispectral LiDAR for the Recovery of Arboreal Parameters," IEEE Trans. Geosci. Remote Sens. **52**(8), 4942–4954 (2014).

[4] McCarthy, A., Collins, R. J., Krichel, N. J., Fernández, V., Wallace, A. M.., Buller, G. S., "Long-range time-of-flight scanning sensor based on high-speed time-correlated single-photon counting," Appl. Opt. **48**(32), 6241 (2009).

[5] Holst, G. C.., Lomheim, T. S., CMOS/CCD Sensors and Camera Systems, Second Edition, SPIE (2007).

[6] El-Desouki, M., Jamal Deen, M., Fang, Q., Liu, L., Tse, F.., Armstrong, D., "CMOS Image Sensors for High Speed Applications," Sensors **9**(1), 430–444 (2009).

[7] Buller, G. S.., Collins, R. J., "Single-photon generation and detection," Meas. Sci. Technol. **21**, 012002 (2010).

[8] Zappa, F., Tisa, S., Tosi, A.., Cova, S., "Principles and features of single-photon avalanche diode arrays," Sens. Actuators Phys. **140**(1), 103–112 (2007).

[9] Cova, S. D.., Ghioni, M., "Single-Photon Counting Detectors," Breakthroughs, 274.

[10] Cova, S., Ghioni, M., Lacaita, A., Samori, C.., Zappa, F., "Avalanche photodiodes and quenching circuits for single-photon detection," Appl. Opt. **35**(12), 1956–1976 (1996).

[11] Cova, S., Tosi, A., Gulinatti, A., Zappa, F.., Ghioni, M., "Avalanche diodes and circuits for infrared photon counting and timing: retrospect and prospect," IEEE LEOS Newsl. **20**(25), 25–28 (2006).

[12] Cova, S., Ghioni, M., Lotito, A., Rech, I.., Zappa, F., "Evolution and prospects for single-photon avalanche diodes and quenching circuits," J. Mod. Opt. **51**(9-10), 1267–1288 (2004).

[13] Lacaita, A., Cova, S., Ghioni, M.., Zappa, F., "Single-photon avalanche diode with ultrafast pulse response free from slow tails," IEEE Electron Device Lett. **14**(7), 360–362 (1993).

[14] Dautet, H., Deschamps, P., Dion, B., MacGregor, A. D., MacSween, D., McIntyre, R. J., Trottier, C.., Webb, P. P., "Photon counting techniques with silicon avalanche photodiodes," Appl. Opt. **32**(21), 3894–3900 (1993).

[15] Bertone, N.., Giudice, A., "Developments in single photon avalanche photodiodes with fast timing resolution," 2006, 611907–611907 – 8.

[16] Zappa, F., Tosi, A., Dalla Mora, A., Guerrieri, F.., Tisa, S., "Single-photon avalanche diode arrays and CMOS microelectronics for counting, timing, and imaging quantum events," 23 January 2010, 76082C – 76082C – 15.

[17] Scarcella, C., Tosi, A., Villa, F., Tisa, S.., Zappa, F., "Low-noise low-jitter 32-pixels CMOS single-photon avalanche diodes array for single-photon counting from 300 nm to 900 nm," Rev. Sci. Instrum. **84**(12), 123112 (2013).

[18] Bronzi, D., Villa, F., Tisa, S., Tosi, A., Zappa, F., Durini, D., Weyers, S.., Brockherde, W., "100000 Frames/s 64 x 32 Single-Photon Detector Array for 2-D Imaging and 3-D Ranging," IEEE J. Sel. Top. Quantum Electron. **20**(6), 354–363 (2014).

[19] Niclass, C., Favi, C., Kluter, T., Gersbach, M.., Charbon, E., "A 128x128 Single-Photon Image Sensor with Column-Level 10-bit Time-to-Digital Converter Array," J. Solid-State Circuits **43**(12), 2977–2989 (2008).
[20] Gersbach, M., Maruyama, Y., Trimananda, R., Fishburn, M. W., Stoppa, D., Richardson, J. A., Walker, R., Henderson, R.., Charbon, E., "A Time-Resolved, Low-Noise Single-Photon Image Sensor Fabricated in Deep-Submicron CMOS Technology," IEEE J. Solid-State Circuits **47**(6), 1394–1407 (2012).
[21] Villa, F., Lussana, R., Bronzi, D., Tisa, S., Tosi, A., Zappa, F., Dalla Mora, A., Contini, D., Durini, D., et al., "CMOS Imager With 1024 SPADs and TDCs for Single-Photon Timing and 3-D Time-of-Flight," IEEE J. Sel. Top. Quantum Electron. **20**(6), 364–373 (2014).
[22] Tyndall, D., Rae, B. R., Li, D. D.-U., Arlt, J., Johnston, A., Richardson, J. A.., Henderson, R. K., "A high-throughput time-resolved mini-silicon photomultiplier with embedded fluorescence lifetime estimation in 0.13 μm CMOS," IEEE Trans. Biomed. Circuits Syst. **6**(6), 562–570 (2012).
[23] Vitali, M., Bronzi, D., Krmpot, A. J., Nikolic, S. N., Schmitt, F.-J., Junghans, C., Tisa, S., Friedrich, T., Vukojevic, V., et al., "A Single-Photon Avalanche Camera for Fluorescence Lifetime Imaging Microscopy and Correlation Spectroscopy," IEEE J. Sel. Top. Quantum Electron. **20**(6), 344–353 (2014).
[24] Field, R. M., Realov, S.., Shepard, K. L., "A 100 fps, Time-Correlated Single-Photon-Counting-Based Fluorescence-Lifetime Imager in 130 nm CMOS," IEEE J. Solid-State Circuits **49**(4), 867–880 (2014).
[25] Zappa, F.., Tosi, A., "MiSPIA: microelectronic single-photon 3D imaging arrays for low-light high-speed safety and security applications," 29 May 2013, 87270L.
[26] Itzler, M. A., Entwistle, M., Owens, M., Patel, K., Jiang, X., Slomkowski, K., Rangwala, S., Zalud, P. F., Senko, T., et al., "Comparison of 32 x 128 and 32 x 32 Geiger-mode APD FPAs for single photon 3D LADAR imaging," 13 May 2011, 80330G – 80330G – 12.
[27] Bronzi, D., Villa, F., Bellisai, S., Tisa, S., Ripamonti, G.., Tosi, A., "Figures of merit for CMOS SPADs and arrays," 2013, 877304–877304 – 7.
[28] Donati, S., Martini, G.., Norgia, M., "Microconcentrators to recover fill-factor inimage photodetectors with pixel on-boardprocessing circuits," Opt. Express **15**(26), 18066–18075 (2007).
[29] Pavia, J. M., Wolf, M.., Charbon, E., "Measurement and modeling of microlenses fabricated on single-photon avalanche diode arrays for fill factor recovery," Opt. Express **22**(4), 4202–4213 (2014).
[30] Dukovic, J., Ramaswami, S., Pamarthy, S., Yalamanchili, R., Rajagopalan, N., Sapre, K., Cao, Z., Ritzdorf, T., Wang, Y., et al., "Through-silicon-via technology for 3D integration," Mem. Workshop IMW 2010 IEEE Int., 1–2 (2010).
[31] Koester, S. J., Young, A. M., Yu, R. R., Purushothaman, S., Chen, K. N., La Tulipe, D. C., Rana, N., Shi, L., Wordeman, M. R., et al., "Wafer-level 3D integration technology," IBM J. Res. Dev. **52**(6), 583–597 (2008).
[32] Itzler, M. A., Entwistle, M., Owens, M., Patel, K., Jiang, X., Slomkowski, K., Rangwala, S., Zalud, P. F., Senko, T., et al., "Design and performance of single photon APD focal plane arrays for 3-D LADAR imaging," 2010, 77801M – 77801M – 15.

[33] Villa, F., Bronzi, D., Zou, Y., Scarcella, C., Boso, G., Tisa, S., Tosi, A., Zappa, F., Durini, D., et al., "CMOS SPADs with up to 500 μm diameter and 55% detection efficiency at 420 nm," J. Mod. Opt. **61**(2), 102–115 (2014).

[34] Villa, F., Markovic, B., Bellisai, S., Bronzi, D., Tosi, A., Zappa, F., Tisa, S., Durini, D., Weyers, S., et al., "SPAD Smart Pixel for Time-of-Flight and Time-Correlated Single-Photon Counting Measurements," IEEE Photonics J. **4**(3), 795–804 (2012).